Energy & Environmental Science

PAPER

Enhanced charge separation in organic photovoltaic films doped with ferroelectric dipoles†

Kanwar S. Nalwa,[a] John A. Carr,[a] Rakesh C. Mahadevapuram,[b] Hari K. Kodali,[c] Sayantan Bose,[d] Yuqing Chen,[a] Jacob W. Petrich,[e] Baskar Ganapathysubramanian[c] and Sumit Chaudhary*[ab]

A key requirement for realizing efficient organic photovoltaic (OPV) cells is the dissociation of photogenerated electron-hole pairs (singlet-excitons) in the donor polymer, and charge-transfer-excitons at the donor–acceptor interface. However, in modern OPVs, these excitons are typically not sufficiently harnessed due to their high binding energy. Here, we show that doping the OPV active-layers with a ferroelectric polymer leads to localized enhancements of electric field, which in turn leads to more efficient dissociation of singlet-excitons and charge-transfer-excitons. Bulk-heterojunction OPVs based on poly(3-hexylthiophene):[6,6]-phenyl-C61-butyric acid methyl ester are fabricated. Upon incorporating a ferroelectric polymer as additive in the active-layer, power conversion efficiencies increase by nearly 50%, and internal quantum efficiencies approach 100% – indicating complete exciton dissociation at certain photon energies. Similar enhancements in bilayer-heterojunctions, and direct influence of ferroelectric poling on device behavior show that improved dissociation is due to ferroelectric dipoles rather than any morphological change. Enhanced singlet-exciton dissociation is also revealed by photoluminescence lifetime measurements, and predicted by simulations using a numerical device model.

[a]*Department of Electrical and Computer Engineering, Iowa State University, Ames, IA, USA. E-mail: sumitc@iastate.edu; Tel: +1 515 294 0606*

[b]*Department of Materials Science and Engineering, Iowa State University, Ames, IA, USA*

[c]*Department of Mechanical Engineering, Iowa State University, Ames, IA, USA*

[d]*Ames Laboratory-USDOE, Iowa State University, Ames, IA, USA*

[e]*Department of Chemistry, Iowa State University, Ames, IA, USA*

† Electronic supplementary information (ESI) available: AFM images, simulation methodology, Raman spectra of photovoltaic films after addition of PVDF-TrFE, Ferroelectric poling results for bilayer devices. See DOI: 10.1039/c2ee03478f

Introduction

Organic photovoltaic (OPV) cells with polymer-fullerene bulk-heterojunction (BHJ) architecture are attracting considerable interest owing to their promise for low-cost solar-electric conversion. Recent progress in power conversion efficiencies of BHJ cells has primarily resulted from the development of materials with tailored energy levels,[1–3] and utilization of annealing and solvent additives to control nano-morphology.[4–9] BHJ cells have now attained power conversion efficiencies of 7–8%, which are impressive, albeit, still lower than the Shockley-Queisser theoretical limit of 21%.[10] This

---

Broader context

Organic photovoltaics are making rapid progress, with their solar-electric power conversion efficiencies now approaching double digits. State-of-the-art organic photovoltaic devices still suffer from several losses or bottlenecks – a major one of them being recombination of photogenerated electron-hole pairs (singlet excitons) within the donor material, or charge-transfer-excitons at the donor–acceptor interface. In this paper, we present a strategy to mitigate this problem – doping the bulk of organic photovoltaic active layers with small amounts of ferroelectric material. Dipoles within the ferroelectric material lead to local enhancements of electric field, which in turn lead to more efficient dissociation of singlet and charge transfer excitons, thus improving the power conversion efficiencies. We believe that in addition to directly impacting the area of organic solar cells, our study also opens the door for investigating more synergies between ferroelectric and conjugated organics – for example, fusion of ferroelectric polymers and conjugated polymers for new paradigms of hybrid piezoelectric, pyroelectric, and photovoltaic devices for energy harvesting from multiple sources.

performance gap is primarily due to losses incurred by insufficient light trapping, parasitic absorption in layers other than the OPV active-layer, singlet-exciton (SE) recombination due to low exciton diffusion lengths, charge-transfer-exciton (CTE) recombination, and low carrier mobilities.[10] Kirchartz et al. estimated that among all loss pathways, SE recombination accounts for nearly 12% efficiency loss, and CTE recombination (geminate and non-geminate) accounts for more than 32% efficiency loss.[10]

In this work, we show that by incorporating ferroelectric dipoles as additives in OPV active layers, both SEs and CTEs can be dissociated more efficiently, leading to enhanced power conversion efficiencies. We used two different OPV structures (BHJ and bilayer) based on a poly(3-hexylthiophene):[6,6]-phenyl-C61-butyric acid methyl ester (P3HT:PCBM) material system to investigate the effect of the ferroelectric co-polymer additive poly(vinylidenefluoride-co-trifluoroethylene) (PVDF-TrFE). We show that the addition of ferroelectric dipoles can significantly improve photovoltaic performance, resulting in ∼52% and ∼60% enhancement of overall power conversion efficiency for BHJ and bilayer cells, respectively. Ruling out other mechanisms using optoelectronic and photophysical characterizations, we show that the performance improvement is due to exciton dissociation being enhanced by the local electric field of ferroelectric dipoles. The efficiency of the BHJ cells improved from 2.5% (for the reference device) to 3.9% upon incorporating PVDF-TrFE additives. The efficiency of our reference device is lower than the best P3HT:PCBM cell efficiencies reported in literature because blend solutions utilized for device fabrication consisted of a low-boiling-point solvent tetrahydrofuran (THF) (25% by volume, 75% being ortho-dicholorbenzene). THF was included because it is a good solvent for PVDF-TrFE, however it is typically not preferred in OPVs due to its fast evaporation rate which leads to suboptimal BHJ morphologies.[11] We expect that exploration of other good or latent solvents of PVDF-TrFE will lead to even higher efficiencies than achieved in this study. Nevertheless, our results unambiguously show that ferroelectric additives (a) lead to improved SE dissociation in morphologies that are otherwise suboptimal in this regard, and (b) also reduce CTE recombination, as evident from internal quantum efficiencies approaching 100% in our BHJ cells.

Recently, Yaun et al. utilized PVDF-TrFE as a buffer layer at the interface of the OPV active-layer and Al cathode, and efficiency enhancement was observed.[12] However, Asadi et al. demonstrated that the performance improvement was insensitive to ferroelectric polarization direction, and was primarily due to increase in open-circuit-voltage (V_{oc}) caused by the improvement of the Al cathode - similar to the effect of alkaline-fluoride buffer layers at the organic/cathode interfaces.[13] In contrast, our report is the first use of a ferroelectric as a helpful additive within the bulk of OPV active-layer. In our ferroelectric doped devices, device performance is clearly influenced by the ferroelectric polarization direction. Also, the performance improvement in our devices is not due to increase in V_{oc} or improvement of the cathode, but rather due to higher short-circuit-current and fill factor resulting from enhanced SE and CTE dissociation, as characterized and discussed below.

Results and discussion

At the outset, we hypothesized that a ferroelectric material embedded in an OPV active-layer can possibly reduce one or more of the aforementioned losses. First, the mismatch of host material's refractive index and the embedded ferroelectric's refractive index can lead to light scattering sites advantageous for optical absorption.[14] Second, the permanent electrical polarization of ferroelectric dipoles can generate localized enhancements of electric field within the active-layer, affecting carrier drift or exciton dissociation or both. According to the modified Braun model[15] (eqn (1)), the probability of ionizing an exciton is a function of electric field strength (E) and binding energy (E_B).

$$\phi(E) = \frac{1}{1 + \frac{\omega_0}{F(E)} e^{\frac{E_B}{kT}}} \quad (1)$$

where $F(E)$ is a function of $e^3 E / 8\pi\varepsilon_0\varepsilon k^2 T^2$. Binding energies of SE and CTE states have been estimated to be in the range of 0.4–0.7 eV and 0.2–0.3 eV, respectively.[16,17] Both energies are an order of magnitude higher than kT at room temperature (∼0.026 eV), making the exponential term in eqn (1) very large. SE excitons that are able to reach the donor–acceptor interface, do indeed decay into a CTE state due to the offset between the lowest unoccupied molecular orbitals of donors and acceptors. However, SEs that do not reach the interface, and CTEs themselves, are still the loss mechanisms, which can be minimized by increased ionization enabled by higher E (eqn (1)). This thought is supported by various studies which show that photocurrent in BHJ OPVs saturates only under a large (>10 V) external reverse bias.[18,19] This implies that complete exciton fission (i.e. all SEs and CTEs) requires an internal electric field of ∼50–70 V μm^{-1}, which is much higher than the field generated by difference in the work-functions of electrodes (typically 1–10 V μm^{-1}). Hence, we expected that ferroelectric dipoles embedded in an OPV active-layer might help in this regard due to their inherent electric field.

We chose PVDF-TrFE for our investigations because it is solution processable, and exhibits a net dipole moment at room temperature.[20] Also, its dielectric constant ($n \sim 11$) is higher than that of organic semiconductors ($n \sim 2$), and thus suitable to test our hypothesis regarding scattering assisted optical absorption. Further, using the classical dipole-field model,[21]

$$E = \frac{4\pi}{\varepsilon} \sigma f \quad (2)$$

where ε is the relative permittivity of PVDF-TrFE, σ is the pyroinduced surface charge density (∼6 μC cm^{-2} for PVDF-TrFE)[22] and f is the volume fraction occupied by the dipoles, we estimated a theoretical enhancement to the device's local internal field to be ∼8*10^3*f V μm^{-1}. A small volume fraction of ∼0.03, for example, corresponds to electric field of ∼240 V μm^{-1}, which is expected to sufficiently dissociate SEs and CTEs.

Four P3HT:PCBM based BHJ cells were fabricated with different amounts of PVDF-TrFE additive (0%, 5%, 10%, and 20% PVDF-TrFE by weight of P3HT). For appropriate comparisons, the final concentration of P3HT:PCBM was kept same (10 mg ml^{-1}) in all four solutions, and each solution had the

same ratio of THF (good solvent for PVDF-TrFE) and *ortho*-dicholorobenzene (ODCB) (1 : 3). On completing the devices, we annealed them at 150 °C to improve the crystallinity of P3HT and PVDF-TrFE. Fig. 1a and Table 1 show the performance of our devices. We observed that short-circuit-current (J_{sc}) and fill factor (*FF*) increase upon the addition of PVDF-TrFE up to 10% concentration, while the V_{oc} of all devices was quite similar.

Next, we set out to test our aforementioned hypotheses and determine the cause(s) behind performance improvement. As shown in Fig. 1b, performance increased as PVDF-TrFE concentration increased from 0% to 5% to 10%. But 20% concentration failed to improve the performance further. We suspected that this was due to aggregation of PVDF-TrFE dipoles. Above some threshold concentration of dipoles, inter-dipole interaction energy increases and leads to aggregation,[21] shielding the electrostatic fields of individual dipoles. Supplementary Fig. S1 shows evidence of this aggregation in the form of PVDF-TrFE agglomerates of size ~100–200 nm. Fig. 1c also shows an indirect evidence in the form of increased light absorption, that can arise from scattering of light due to refractive index mismatch between PVDF-TrFE agglomerates and P3HT:PCBM. Films with 5% and 10% PVDF-TrFE showed lower light absorption than the films with 20% concentration due to less or no scattering. They also showed less absorption than the film with 0% concentration because part of their active-layer is occupied by wide bandgap PVDF-TrFE, which does not absorb visible light. Thus, improved performance in devices with 5% and 10% PVDF-TrFE cannot be attributed to optical effects.

Table 1 Effect of PVDF-TrFE concentration on the photovoltaic parameters of BHJ OPVs

	J_{sc} (mA cm^{-2})	V_{oc} (V)	*FF*	*Efficiency*
0% PVDF-TrFE	9.6	0.55	48	2.5%
5% PVDF-TrFE	10.4	0.55	54	3.1%
10% PVDF-TrFE	11.3	0.57	60	3.9%
20% PVDF-TrFE	10.2	0.57	55	3.2%

Using the model presented in eqn (2), we estimated internal electric field enhancement to be ~150 V μm^{-1} and ~300 V μm^{-1} for the devices with 5% and 10% PVDF-TrFE concentration. To investigate the effect of the dipoles' field direction on charge transport, we measured *J–V* characteristics after poling the ferroelectric (Fig. 1d–f). A 20 V pulse of 10 ms duration was applied on the ITO electrode with both positive and negative polarities, and *J–V* characteristics were measured again. The applied field (~ ±110 MV m^{-1}) correlates well with the PVDF-TrFE polarization *vs.* electric field data reported in literature; coercive field of ~50 MV m^{-1} and a saturation field (*i.e.* 100% polarization) of ~100 MV m^{-1} are generally reported.[23,24] For the control devices without PVDF-TrFE, *J–V* curves did not change after applying a pulse of either polarity, as expected. Devices with 20% PVDF-TrFE also showed no effect of poling, offering another evidence of dipole-aggregation discussed above. In contrast, for the devices with 5% and 10% PVDF-TrFE, a negative 20 V pulse (negative poling) significantly reduced V_{oc}
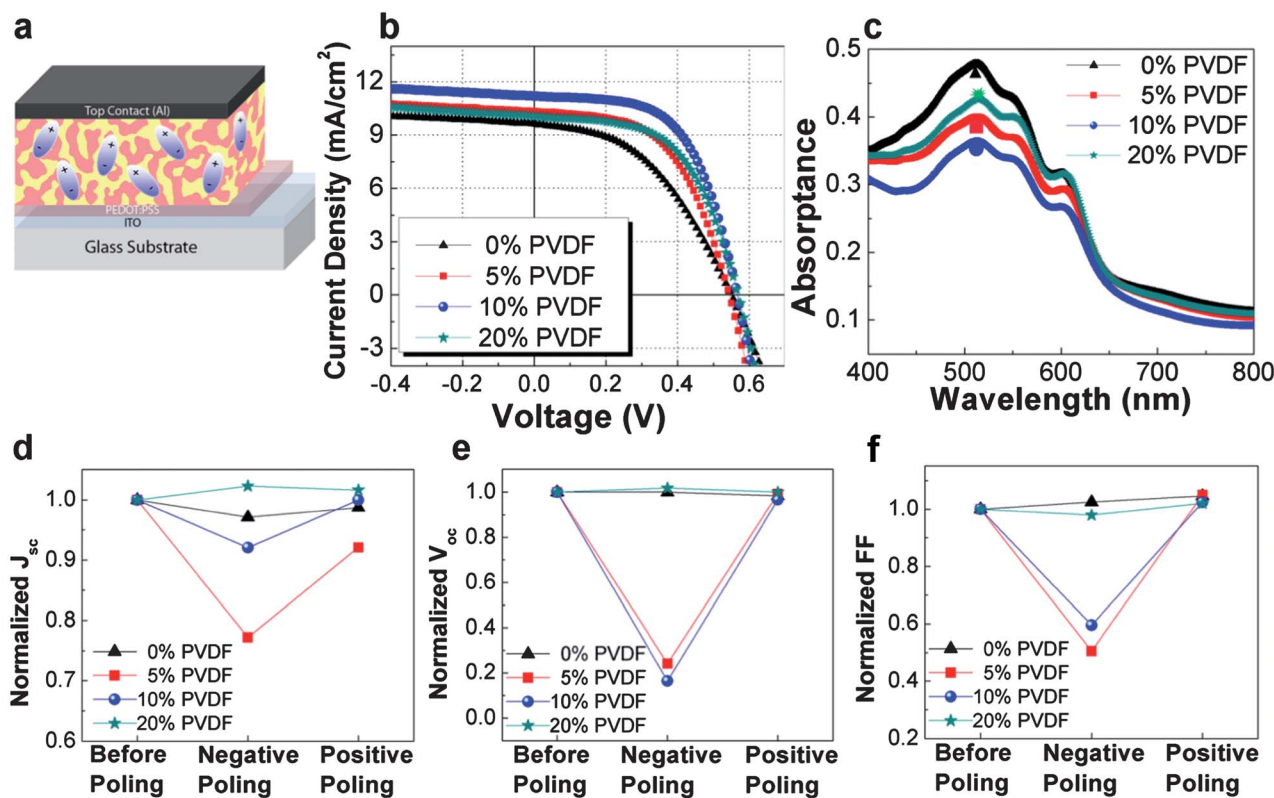

Fig. 1 Effect of PVDF-TrFE dipole addition on the performance of the BHJ OPVs. (a) schematic of BHJ cells in which active layer is doped with PVDF-TrFE. (b) photocurrent density *versus* voltage curves, and (c) absorption of the photoactive blend layer. Effect of poling on (d) short-circuit current, (e) open circuit voltage, and (f) fill factor of OPVs with and without PVDF-TrFE additives.

7044 | *Energy Environ. Sci.*, 2012, **5**, 7042–7049

This journal is © The Royal Society of Chemistry 2012

and FF, and to some extent J_{sc}, while a subsequent positive pulse (positive poling) restored the original performance. Positively poled device, however, showed the same performance as the unpoled device. One should note that positively poled dipoles have electric field in the same direction as built-in field due to the difference in electrodes' work-functions. Above observations enable the following deductions: (i) since the device performance degrades in case of negative poling, the efficiency enhancing mechanism in positively poled or unpoled devices must be operative in the bulk of the active-layer rather than at the organic-electrode interface. If the case was latter, polarization direction will not have any effect on the device as demonstrated by Asadi et al.;[13] (ii) either the efficiency enhancing mechanism is equally strong for random dipoles and positively poled dipoles, or the dipoles are already aligned favorably in the unpoled device; (iii) efficiency enhancement is not due to improved charge transport alone because positive poling does not improve the unpoled device, and the negative poling degrades the device performance too severely. Considering that PVDF-TrFE dipoles occupy as low as 5% volume fraction in the active-layer, it is highly unlikely that such a severe degradation will originate from reduced charge transport alone. Thus, the efficiency enhancement in 5% and 10% PVDF-TrFE devices seems to be more likely a result of enhanced exciton (SE or CTE or both) dissociation, as the increased electric field around the dipoles can assist electron-hole separation even in an unpoled device with randomly-oriented dipoles.

Simulations using a one-dimensional device model support the above argument about additive dipoles enhancing exciton dissociation. For these simulations, we assumed a dipole of length 10 nm placed at the center of a 100 nm thick active-layer, with positive and negative charges concentrated at opposite ends (see supplementary information for detailed simulation methodology). Computations reveal the effect of dipole addition on the voltage and electric field profiles inside the active-layer, at short circuit condition (Fig. 2). The case of 'Dipole orientation -1'– which represents negatively poled ferroelectric – exhibits a decrease in the slope of voltage profile, thus lowering of electric field in the region surrounding the dipole. The decrease in electric field reduced the exciton dissociation rate constant (k_d) by $\sim$9% (averaged across the active-layer thickness) (Fig. 2c), according to the equation:

$$k_d = \frac{3R}{4\pi a^3} e^{-E_B/k_B T}\left(1 + b + b^2/3 + ...\right) \qquad (3)$$

where $b = e^3 E/8\pi\varepsilon_0\varepsilon k^2 T^2$. Lower k_d implies lower probability of exciton dissociation, resulting in loss of carriers, and causing partial decrease in V_{oc} and FF as seen in the negatively poled devices. However, in the case of 'Dipole orientation $+1$', the slope of voltage profile and thus the electric field in the active layer increased, thereby enhancing k_d by 12%.

To experimentally validate the exciton dissociation aspect, we measured external quantum efficiency (EQE) of our devices for the wavelength range of 400 nm–800 nm (Fig. 3a). Trends are the same as in J–V curves, as expected. However, since the active-layers of our devices exhibited significant variation in optical absorption, EQE cannot be considered representative of enhanced exciton dissociation. Hence, internal quantum efficiency (IQE) was calculated using the method detailed by Burkhard et al.,[25] and is shown in (Fig. 3b). The IQE curves are not flat because excitons generated at different photon energies are not harnessed equally efficiently. Harnessing of PCBM excitons has been reported to be quite inefficient,[26] which explains the lower IQE at lower wavelengths, where PCBM is the dominant light absorber. For devices with 10% PVDF-TrFE, IQE approached 100% at higher wavelengths, implying almost complete dissociation of SEs and CTEs. It also indicates that SEs unable to reach the P3HT:PCBM interface also undergo dissociation due to local field of dipoles. We further probed exciton dynamics of the active-layers using photoluminescence (PL) lifetime measurements. As shown in Fig. 3c, the PL lifetimes were found to be 100 ps, 95 ps, 73 ps and 122 ps for the active-layers with 0%, 5%, 10% and 20% PVDF-TrFE. Clearly, the active-layer with 5% and 10% PVDF-TrFE exhibit shortened PL lifetimes, indicative of higher SE dissociation. PL lifetime of the active-layer with 20% PVDF-TrFE, however, was higher than the control. AFM images (Fig. S4) show a coarser morphology of the films with 20% PVDF-TrFE in areas not containig any PVDF agglomerates. This could result from bigger P3HT domains in the active-layer, indicating that donor–acceptor morphology can be altered by the inroduction of the ferroelectric. This raises an important question: could it be that active-layers with 5% and 10% PVDF-TrFE somehow have a more favorable phase separation that is leading to more efficient SE quenching and better PV performance?
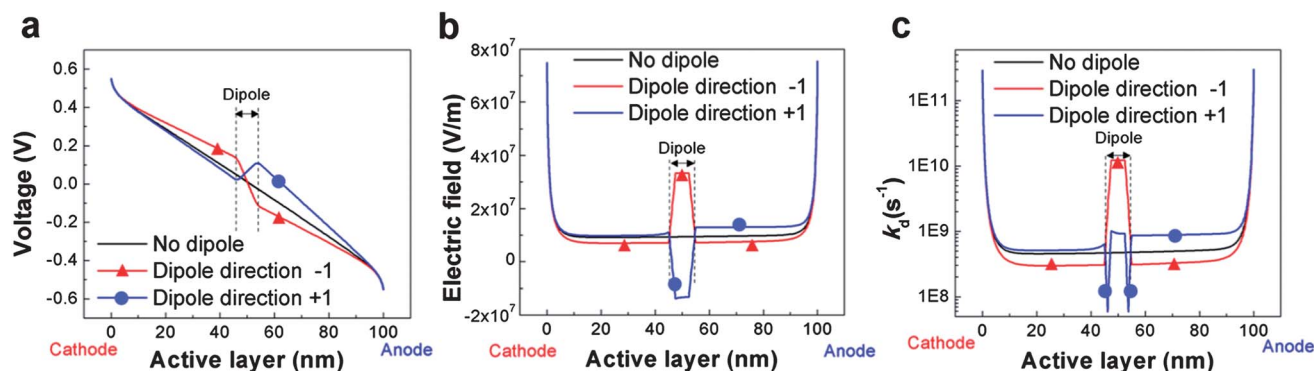

Fig. 2 Simulated effect of a dipole additive on voltage (a), electric field (b), and exciton dissociation contant k_d (c) at short-circuit condition, for three conditions: no dipole, dipole orientation -1 i.e. dipole vector from cathode to anode and dipole orientation $+1$ i.e. dipole vector from anode to cathode.
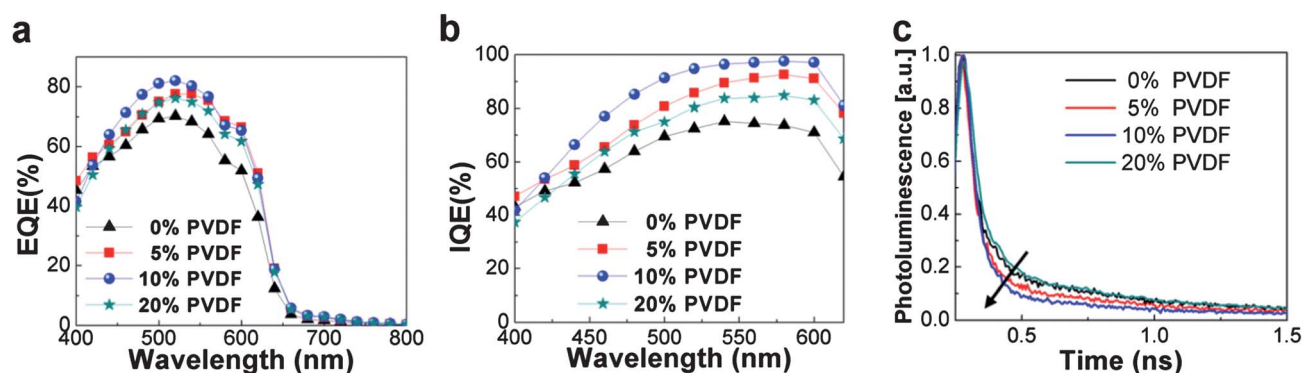
Fig. 3 External quantum efficiency (EQE) (d), internal quantum efficiency (IQE) (e), and photoluminescence lifetime (f) plots of P3HT:PCBM BHJ devices with PVDF-TrFE additives. Arrow shows order of decreasing lifetimes (20% > 0% > 5% > 10%).

AFM images did not reveal any distinct differences between the morphologies of active-layers with 0%, 5% and 10% PVDF-TrFE. Raman spectra also did not show any change in P3HT crystallinity upon adding PVDF-TrFE (Fig. S5). However, for more certain elucidation, we decided to use bilayer-hetero-junction device architecture as a vehicle to eliminate the possible effects of morphology. We investigated the effect of PVDF-TrFE on bilayer devices with P3HT and PCBM as adjacent layers deposited from orthogonal solvents. We examined three types of bilayer P3HT:PCBM OPV devices (Fig. 4a–c): (i) control – a bilayer P3HT:PCBM device; (ii) mixture – a bilayer P3HT:PCBM device with 10 wt% PVDF-TrFE additive in the P3HT layer, and (iii) interfacial – technically a tri-layer device, that included a thin PVDF-TrFE layer sandwiched between P3HT and PCBM layers. These three structures allowed us to investigate where the ferroelectric dipoles are most beneficial – in the P3HT domains, or at P3HT:PCBM interface. The performance characteristics of these cells showed distinct differences (Fig. 4d and Table 2). With 10% PVDF-TrFE additive in the P3HT layer of P3HT:PCBM bilayer cells, we again observed 42% and 15% increase in J_{sc} and FF, respectively, compared to the control bilayer cell without PVDF-TrFE (Fig. 4 and Table 2). Though the bilayer morphologies cannot be considered truly bilayer due to the evidence of interdiffusion reported in literature,[27] nevertheless, it cannot be expected that the bilayer device with PVDF-TrFE mixed in P3HT will have a more BHJ-type nature than the control. In fact, it should be quite to the contrary because the presence of PVDF-TrFE sites should reduce the intercalation of PCBM into P3HT domains. Thus, it can be confidently asserted that a better nanomorphology is not the reason behind better performance of the bilayer devices with PVDF-TrFE additives, and the enhanced exciton dissociation and performance improvement is indeed due to local ferroelectric fields. Similar claim can then be extended to BHJ devices as well, as absorption and transport have already been ruled out as performance enhancing mechanisms.

The interfacial device exhibited 16% decrease and 25% increase in J_{sc} and V_{oc}, respectively, compared with the control device. Both changes in the interfacial device can be imputed to the presence of ferroelectric interfacial layer acting as a barrier that reduces the electronic coupling between P3HT and PCBM. This in turn (a) reduces the reverse saturation current and increases

V_{oc},[28] and (b) impedes charge transfer from P3HT to PCBM, thus decreasing J_{sc}. These results and the improvements observed in BHJ cells indicate that for BHJ cells also, ferroelectric dipoles must be primarily in the P3HT domains rather than at the P3HT-PCBM interface. Some dipoles in PCBM domains are also possible. Fig. 4e shows that the mixture device displayed approximately 60%–100% improvement in EQE in the wavelength range 425 nm–625 nm, as compared with the control. We also investigated the dependence of EQE on reverse bias. In OPVs, reverse bias improves carrier transport as well as exciton dissociation. Fig. 3f shows the EQE ratio of unbiased devices to biased devices (at −1V) for all three bilayer OPVs. One can see that the control device exhibited the highest improvement during a −1 V biasing (nearing 1.5) while the mixture device displayed the lowest (nearing 1.2). This implies that at short-circuit condition, the control device exhibits poorer SE quenching due to insufficient internal field in the P3HT phase, while the mixture device already has more efficient SE quenching due to the local field of ferroelectric dipoles. This shows that ferroelectric alleviates OPVs' performance dependence on exciton diffusion length, when introduced as additive in donor polymers.

We also probed the exciton dynamics of bilayer structures using PL lifetime measurements, and they clearly show enhanced SE dissociation upon incorporating PVDF-TrFE (Fig. 3g). The normalized PL lifetimes were found to be 144 ps, 122 ps, and 66 ps for the control, mixture, and interfacial devices respectively. The mixture device exhibited a ~15% decrease in PL lifetime when compared with the control device, showing less radiative recombination of SEs. Previous reports have shown evidence of field-assisted dissociation of the SE in organic films, where fluorescence quenching increased as a function of applied field strength.[29] Using eqn (2), we estimate an increment in electric field as high as 600 V μm^{-1} in the mixture device. Surprisingly, the interfacial structure exhibited a much larger reduction in PL lifetime (~54% over the control, and even more than the BHJ structures). The reason for this is not yet clear. Presently, we speculate that there is a higher density of radiatively decaying SEs near the surface of P3HT films, while in the bulk more SEs decay non-radiatively due to microcrystalline lamellar stacking or concentration quenching. PL lifetime measurements only reflect the fate of radiatively decaying SEs, which, according to the above speculation, will be more severely affected in the
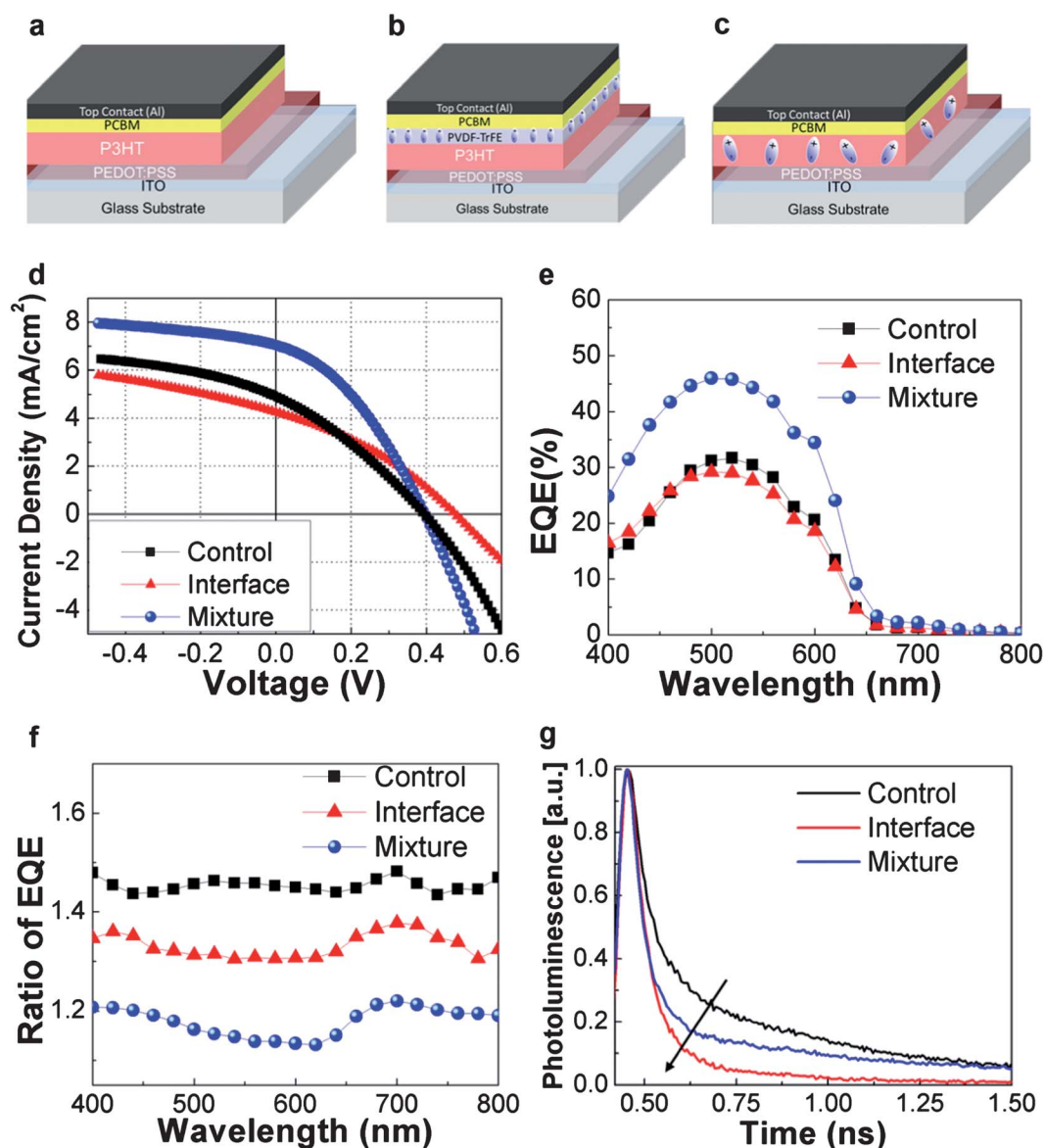
7046 | *Energy Environ. Sci.*, 2012, **5**, 7042–7049

This journal is © The Royal Society of Chemistry 2012

Fig. 4 Performance of P3HT:PCBM bilayer OPVs with PVDF-TrFE as additive in P3HT layer and as an interfacial layer between P3HT and PCBM layers. (a–c), schematic diagrams of three types of devices fabricated. (d) Photocurrents of P3HT:PCBM bilayer control cells, and cells with PVDF-TrFE as interfacial layer (interface device) and as additive in the P3HT layer (mixture device). Also shown for these three types of devices are: (e) External quantum efficiency (EQE) as a function of wavelength; (f) Ratio of EQE at −1 V and 0V bias. (g) PL lifetime plots for the three types of structures. Arrow shows order of decreasing lifetimes (control > mixture > interface).

Table 2 Effect of PVDF-TrFE placement on the photovoltaic parameters of bilayer OPVs

	J_{sc} (mA cm^{-2})	V_{oc} (V)	FF	Efficiency
Control bilayer	5	0.4	39	0.8%
Mixture bilayer	7.1	0.4	45	1.3%
Interface bilayer	4.2	0.5	35	0.7%

interfacial case than in the mixture case. If the above speculation is true, we can confidently say that in the mixture device and BHJ devices, ferroelectric dipoles help to harness both types of SEs, ones that will otherwise decay radiatively, or non-radiatively.

Conclusions

In summary, we showed that a ferroelectric additive in the bulk of OPV active-layers leads to better device performance due to higher photocurrent and fill-factor. Optical absorption, and dependence of device performance on ferroelectric-poling revealed that the optical effects and improved charge transport, respectively, are not the improvement mechanisms. Upon addition of PVDF-TrFE, IQE of BHJ devices approached 100% for some wavelengths, which meant near complete exciton (SE and CTE) harvesting at these photon energies. Enhanced SE dissociation was also predicted by device simulations and verified by PL lifetime measurements. Efficiency and exciton-dissociation

enhancement was also observed for bilayer OPVs with PVDF-TrFE additive in the P3HT layer, which showed that observed enhancements do not have their origin in morphological changes. Thus, our investigations show that utilizing ferroelectrics as additives is a promising methodology for alleviating the dependence of OPV performance on short SE diffusion lengths, and CTE recombination.

Experimental

Anode preparation

Indium-doped tin oxide (ITO; Delta Technologies) coated glass slides were cleaned by sonication in isopropanol, acetone, detergent, ethanol, methanol, and deionized water. The ITO substrates were then blown dry with nitrogen and exposed to air plasma (Harrick Scientific) for 5 min. A poly(ethylenedioxythiophene):poly(styrenesulfonic acid) (PEDOT:PSS; H C Stark) film was spin-coated (3,000 rpm for 60 s) onto the treated substrates, and the casted films were annealed on a hot plate at 120 °C for 10 min.

Fabrication of BHJ OPVs

Three solutions were prepared of PVDF-TrFE copolymer (70 : 30 mol%; PiezoTech) in tetrahydrofuran (THF; Sigma-Aldrich) with concentrations 2mg ml⁻¹, 4mg ml⁻¹ and 8mg ml⁻¹. The donor–acceptor blend with 1 : 1 weight ratio (P3HT:PCBM; NANO C, Inc.) and 13.33 mg ml⁻¹ concentration in *ortho*-Dichlorobenzene (ODCB; Sigma-Aldrich) was used. 0.25 ml of pure THF and 3 PVDF-TrFE solutions (2, 4 and 8mg ml⁻¹) in THF were mixed with 0.75 ml of blend solution to get 4 solutions with 0, 5, 10 and 20% PVDF by weight of P3HT. This allowed to have final concentration of P3HT:PCBM same (10mg ml⁻¹) in all 4 solutions, with each solution having same ratio of THF and ODCB solvents (1 : 3) to ensure appropriate comparison. The solvent mixtures was required because PVDF-TrFE does not dissolve in ODCB, and hence was dissolved in THF and then mixed with the blend solution in 3 different concentrations. The solutions were magnetically stirred for several hours at 45 °C. The solutions were then spin coated at 600 rpm for 40 s over PEDOT:PSS layer and dried at room temperature under a petri dish. Finally, Al (100 nm) cathode was deposited by thermal evaporation, and devices were annealed at 150 °C for 2 min.

Fabrication of bilayer OPVs

First, two solutions (PS1 and PS2) were prepared (for subsequent use in making a next set of solutions) in an argon atmosphere: PS1 consisted of P3HT in ODCB at a concentration of 26.67 mg ml⁻¹ and PS2 comprised PVDF-TrFE in THF at a concentration of 8mg mL⁻¹. Next, four film solutions (FS1, FS2, FS3 and FS4) were made (for depositing OPV layers). FS1 consisted 0.75 ml of PS1 mixed with 0.25 ml of PS2 to give a P3HT(ODCB):PVDF-TrFE(THF) ratio of 20 : 2. FS2 comprised of 0.75 ml of PS1 mixed with 0.25ml THF to give 20 mg mL⁻¹ P3HT:(ODCB + THF). FS3 contained PCBM in dicholoromethane at a concentration of 10 mg mL⁻¹. FS4 included PVDF in dimethylformamide at a concentration of 2mg mL⁻¹. FS1/FS2, FS3 and FS4 were heated to 45 °C, 0 °C and 65 °C, respectively, and

magnetically stirred for several hours. After being cooled to room temperature, the P3HT solutions (FS1 and FS2) were then filtered and spin-cast at 1,000 rpm for 90 s onto the dried PEDOT:PSS coated ITO films, producing a film thickness of ~115 nm. For the three devices presented here, (i) the control device, (ii) the mixture device and (iii) the interface device, FS2, FS1 and FS2 solutions were casted, respectively. The films were then covered with a petri dish and allowed to dry for ≥ 10 min. FS4 was then filtered and spun at 4,000 rpm for 60 s onto the P3HT:(ODCB + THF) layer of the interface device, producing an interfacial film thickness of <10 nm. This film was then annealed on at 150 °C for 1 min. The device was again covered and the interface film was allowed to cool. FS3 was then filtered and spin-cast (4,000 rpm for 10 s) to a thickness of ~34 nm onto all three devices and was immediately annealed at 150 °C for 1 min. After allowing the films to cool, a ~100 nm thick Al cathode was evaporated on all devices at a rate <5 Å s⁻¹.

Photovoltaic characterization

J–V characterization was done using ELH Quartzline halogen lamp, the intensity of which was calibrated using a crystalline Si cell with a KG-5 filter. EQE measurements were also done using this lamp and a monochromator with a lock-in amplifier. The reference was a calibrated Si photodiode with known EQE spectra. To calculate IQE of the BHJ devices, all the films for absorption measurement were spun cast on glass substrates. The absorption spectra were measured in Varian Cary 5000 UV-Vis-NIR spectrophotometer.

Time resolved photoluminescence experiments

Excited-state PL-lifetime measurements were performed using the set-up described elsewhere.[30] Briefly, a homebuilt mode-locked Ti:sapphire oscillator pumped by a Nd:VO4 laser (Millennia, Spectra Physics) producing femtosecond pulses tunable from 780 to 900 nm with a repetition rate of 82 MHz was used as the laser source. The fundamental wavelength at 814 nm from the Ti:sapphire oscillator was modulated by a Pockels cell (Model 350-160, Conoptics Inc.) to reduce the repetition rate to approximately 8.8 MHz and was subsequently frequency-doubled by using a harmonic generator (Model TP- 2000B, U-Oplaz Technologies). The resulting blue light, which had a central wavelength of 407 nm, provided the excitation source, and emission (λ > 505 nm) was collected in front face geometry from solid films using appropriate filters to eliminate possible interference from scattered light. The full width at half-maximum of the instrument response function was ~35 ps. All of the measurements were made in a 3.33 ns time window with a total of 1024 channels. A total of 65530 counts were collected at the peak channel for all of the lifetime measurements.

Acknowledgements

Notes and references

1 H. Y. Chen, J. H. Hou, S. Q. Zhang, Y. Y. Liang, G. W. Yang, Y. Yang, L. P. Yu, Y. Wu and G. Li, *Nat. Photonics*, 2009, **3**, 649–653.

2 Y. Y. Liang, Z. Xu, J. B. Xia, S. T. Tsai, Y. Wu, G. Li, C. Ray and L. P. Yu, *Adv. Mater.*, 2010, **22**, E135–E138.

3 S. H. Park, A. Roy, S. Beaupre, S. Cho, N. Coates, J. S. Moon, D. Moses, M. Leclerc, K. Lee and A. J. Heeger, *Nat. Photonics*, 2009, **3**, 297–U295.

4 G. Li, V. Shrotriya, J. S. Huang, Y. Yao, T. Moriarty, K. Emery and Y. Yang, *Nat. Mater.*, 2005, **4**, 864–868.

5 G. Li, Y. Yao, H. Yang, V. Shrotriya, G. Yang and Y. Yang, *Adv. Funct. Mater.*, 2007, **17**, 1636–1644.

6 W. L. Ma, C. Y. Yang, X. Gong, K. Lee and A. J. Heeger, *Adv. Funct. Mater.*, 2005, **15**, 1617–1622.

7 J. Peet, J. Y. Kim, N. E. Coates, W. L. Ma, D. Moses, A. J. Heeger and G. C. Bazan, *Nat. Mater.*, 2007, **6**, 497–500.

8 Y. Yao, J. H. Hou, Z. Xu, G. Li and Y. Yang, *Adv. Funct. Mater.*, 2008, **18**, 1783–1789.

9 S. Miller, G. Fanchini, Y. Y. Lin, C. Li, C. W. Chen, W. F. Su and M. Chhowalla, *J. Mater. Chem.*, 2008, **18**, 306–312.

10 T. Kirchartz, K. Taretto and U. Rau, *J. Phys. Chem. C*, 2009, **113**, 17958–17966.

11 J. Liu, Y. J. Shi and Y. Yang, *Adv. Funct. Mater.*, 2001, **11**, 420–424.

12 Y. B. Yuan, T. J. Reece, P. Sharma, S. Poddar, S. Ducharme, A. Gruverman, Y. Yang and J. S. Huang, *Nat. Mater.*, 2011, **10**, 296–302.

13 K. Asadi, P. de Bruyn, P. W. M. Blom and D. M. de Leeuw, *Appl. Phys. Lett.*, 2011, **98**, 183301.

14 Z. Zhou, R. Shinar, A. J. Allison and J. Shinar, *Adv. Funct. Mater.*, 2007, **17**, 3530–3537.

15 M. Wojcik and M. Tachiya, *J. Chem. Phys.*, 2009, **130**, 104107.

16 C. Deibel, D. Mack, J. Gorenflot, A. Scholl, S. Krause, F. Reinert, D. Rauh and V. Dyakonov, *Phys Rev B*, 2010, **81**.

17 X. Y. Zhu, Q. Yang and M. Muntwiler, *Acc. Chem. Res.*, 2009, **42**, 1779–1787.

18 V. D. Mihailetchi, L. J. A. Koster, J. C. Hummelen and P. W. M. Blom, *Phys. Rev. Lett.*, 2004, **93**, 216601.

19 P. Peumans, A. Yakimov and S. R. Forrest, *J. Appl. Phys.*, 2003, **93**, 3693–3723.

20 Z. Y. Cheng and Q. M. Zhang, *MRS Bull.*, 2008, **33**, 183–187.

21 D. Shvydka and V. G. Karpov, *Appl. Phys. Lett.*, 2008, **92**, 053507.

22 K. H. Lee, G. Lee, K. Lee, M. S. Oh, S. Im and S. M. Yoon, *Adv. Mater.*, 2009, **21**, 4287–4291.

23 M. Wegener, *Rev. Sci. Instrum.*, 2008, **79**, 106103.

24 R. Naber, B. De Boer, P. Blom and D. De Leeuw, *Appl. Phys. Lett.*, 2005, **87**, 203509.

25 G. F. Burkhard, E. T. Hoke and M. D. McGehee, *Adv. Mater.*, 2010, **22**, 3293–3297.

26 G. F. Burkhard, E. T. Hoke, S. R. Scully and M. D. McGehee, *Nano Lett.*, 2009, **9**, 4037–4041.

27 K. H. Lee, P. E. Schwenn, A. R. G. Smith, H. Cavaye, P. E. Shaw, M. James, K. B. Krueger, I. R. Gentle, P. Meredith and P. L. Burn, *Adv. Mater.*, 2011, **23**, 766.

28 K. Vandewal, K. Tvingstedt, A. Gadisa, O. Inganas and J. V. Manca, *Nat. Mater.*, 2009, **8**, 904–909.

29 M. I. Khan, G. C. Bazan and Z. D. Popovic, *Chem. Phys. Lett.*, 1998, **298**, 309–314.

30 S. Bose, R. Adhikary, P. Mukherjee, X. Y. Song and J. W. Petrich, *J. Phys. Chem. B*, 2009, **113**, 11061–11068.

This journal is © The Royal Society of Chemistry 2012

Energy Environ. Sci., 2012, **5**, 7042–7049 | 7049